POLITECNICO DI TORINO
Repository ISTITUZIONALE

P2-Type Na0.84Li0.1Ni0.27Mn0.63O2Layered Oxide Na-Ion Battery Cathode: Structural Insights and
Electrochemical Compatibility with Room-Temperature Ionic Liquids

Terms of use:

(Article begins on next page)

18 December 2024

Article

P2-Type Na$_{0.84}$Li$_{0.1}$Ni$_{0.27}$Mn$_{0.63}$O$_2$-Layered Oxide Na-Ion Battery Cathode: Structural Insights and Electrochemical Compatibility with Room-Temperature Ionic Liquids

Arianna Massaro, Gabriele Lingua, Francesco Bozza, Alessandro Piovano, Pier Paolo Prosini, Ana B. Muñoz-García, Michele Pavone,* and Claudio Gerbaldi*

Cite This: *Chem. Mater.* 2024, 36, 7046−7055

Read Online

ACCESS | Metrics & More | Article Recommendations | Supporting Information

ABSTRACT: Modern technologies that can replace state-of-the-art Li-ion batteries (LIBs), such as Na-ion batteries (NIBs), are currently driving new advancements in energy storage research. Developing functional active materials having sustainable features and enhanced performances able to assess their exploitation in the large-scale market represents a major challenge. Rationally designed P2-type layered transition metal (TM) oxides can enable high-energy NIB cathodes, where the tailored composition directly tunes the electrochemical and structural properties. Such positive electrodes need stable electrolytes, and exploration of unconventional room-temperature ionic liquid (RTIL)-based formulations paves the route toward safer options to flammable organic solvents. Notwithstanding the fact that Li$^+$ doping in these materials has been proposed as a viable strategy to improve structural issues, an in-depth understanding of structure−property relationship as well as electrochemical testing with innovative RTIL-based electrolytes is still missing. Herein, we propose the solid-state synthesis of P2-Na$_{0.84}$Li$_{0.1}$Ni$_{0.27}$Mn$_{0.63}$O$_2$ (NLNMO) cathode material, which exhibits promising structural reversibility and superior capacity retention upon cycling when tested in combination with RTIL-based electrolytes (EMI-, PYR$_{14}$-, and N$_{1114}$-FSI) compared to the standard NaClO$_4$/PC. As unveiled from DFT calculations, lattice integrity is ensured by the reduced Jahn−Teller distortion upon Na removal exerted by Mn^{4+} and Li$^+$ sublattices, while the good redox reversibility is mainly associated with the electrochemically active Ni^{2+}/Ni^{3+}/Ni^{4+} series burdening the charge compensation upon desodiation. By declaring the electrochemical compatibility of the P2-NLNMO cathode with three RTIL-based electrolytes and dissecting the role of Li/Ni/Mn sublattices in determining the electrochemical behavior, our comprehensive study enlightens the potential application of this electrode/electrolyte setup for future high-energy NIB prototype cells.
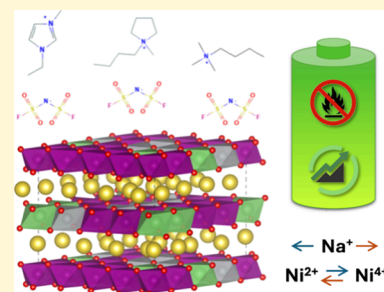
1. INTRODUCTION

Research in secondary batteries is being enriched over past decades by dynamic development of different chemistries and systems, as well as the optimization of related active materials and their operating principles.[1] Since the pioneering Li-ion batteries (LIBs) have been powering all modern portable electronic devices and electricity-propelled vehicles, Na-ion batteries (NIBs) with cell configuration and working mechanisms similar to LIBs have emerged as ideal alternatives, likely but not exclusively, for large-scale energy storage systems.[2,3] The advantage of NIBs mainly resides in the remarkable cost reduction of raw materials, comprising either the sodium resources abundantly distributed in Earth's crust and the less expensive transition metals (e.g., manganese, nickel, and iron) solely required to fabricate high-performance cathode materials.[4] The unprecedented demand for lithium and other critical materials has driven new frontiers of energy storage toward sustainability and triggered the commercialization of NIBs as promising post-lithium technology.[5] Besides, cost reduction, increased energy density and improved cycling stability as well as safety are highly pursued features, which

have put layered sodium TM oxides (Na$_x$TMO$_2$) in the spotlight of advanced cathode research.[6] Several key aspects still characterize this family of materials, including irreversible phase transformations during cycling, poor air stability, and complex charge-compensation mechanisms.[7] Fundamental understanding of degradation behavior upon cycling and air exposure,[8] correlating structure-performance relationships, and establishing general design strategies must be considered for their effective exploitation in commercial NIBs.[9] Recent progress in this field has highlighted critical factors that would balance the overall material efficiency.[10] General consensus exists on the key role of chemical composition at TM sites, where both ratio and nature of involved TM redox

couples are known to sensibly affect the phase stability and structural retention during subsequent Na insertion/extraction from the layered lattice.[11,12] How the Na_xTMO_2 stoichiometry determines the physicochemical properties as well as the electrochemical response is decisive for the cell performance.[13] In particular, Mn- and Ni-containing Na_xTMO_2 have been frequently investigated because of the enhanced energy density resulting from high operating potential and relatively large reversible capacity.[14−17] However, P2 polymorphs usually exhibit staircase potential curves due to multiple phase transitions upon Na-ion insertion and extraction, which lead to decreased cycling stability. To suppress severe structure transformation, Li^+ can be introduced to partially substitute Ni^{2+} in the TM layer thanks to similar ionic radius.[18,19] Simultaneously, lithium ions also enter intrinsic Na^+ vacancies in the Na layer, which results in the disruption of Na^+/vacancy ordering of the more stabilized structure.[20] Several Li-substituted Na_xTMO_2-layered oxides have been investigated, with a promising specific capacity of 100−120 mAh g^{-1} achieved in the 2.0−4.2 V potential range[18,21,22] and stable cycling for 50 cycles.[19] Structural benefits in Li-doped Na_xTMO_2 also comprise the steady and long-term cycling that can be achieved at a relatively high voltage range,[23] which is usually characterized by subtle irreversible oxygen evolution processes. Generally embodying a debated topic, the anionic redox activity can represent a source of additional energy density, provided that the tunable and controlled evolution of oxide oxidation reactions can prevent undesired side effects of structure collapse.[24−26]

From a practical point of view, the current synthetic procedures have made significant progress in terms of handling and tunability of the resulting structures. These layered oxides can be usually prepared by different approaches, including coprecipitation of the $TM(OH)_2$ produced by controlled titration of TM nitrates with NaOH solution,[19] sintering of $TM(OH)_2$ nanoplate precursors and alkali metal carbonates,[27] or solid-state reactions employing carbonates and oxides of corresponding TM and alkali metals.[18,28] The solid-state method is one of the most widely used approaches for the production of active electrode materials. It typically includes mixing of the starting materials and heating of precursors, followed by annealing or quenching, thus allowing to achieve high degrees of crystallinity, low defect concentration, and highly pure phases.[29] While a general picture for the design and production of efficient Na_xTMO_2 materials with desired properties is rapidly taking shape, the predictive power of computational approaches can be helpful in assisting the experimental investigations.[13] By gaining access to the electronic structure of materials, *ab initio* simulations can unveil the mechanistic details of sodiation/desodiation at the nanoscale, outline rational descriptors to predict main properties from the chemical structure, and identify driving factors toward the optimization of required features (i.e., stabilization of oxygen electron holes, suppression of TM interlayer migration, and increased TM−O bond covalency).[30−38] To our knowledge, advanced characterization studies on P2-type layered Li-doped Na_xTMO_2 are at an early stage, while the emerging interest for efficient and stable NIB cathodes would call for wide investigations of their underlying properties, as well as ultimate application in real devices. So far, electrochemical testing has been solely carried out with conventional electrolytes, such as aprotic solutions of $NaPF_6$ or $NaClO_4$ salts in organic carbonates.[18,19,27,28] Exploring the

compatibility with innovative RTIL-based electrolytes would undoubtedly meet the safety and sustainability requirements established for the new generation battery targets.[39,40] As low-volatile and essentially nonflammable organic salts with extremely low melting points, RTILs are highly structured fluids composed of large and soft cations and anions, the chemical and physical properties of which can be tuned depending on the adopted composition (as reported in the literature).[41] Among many investigated combinations, pyrrolidinium (PYR)- and imidazolium (EMI)-based cations, with bis(trifluoromethanesulfonyl) and bis(fluorosulfonyl) imides, namely, TFSI and FSI anions, are the most widely adopted in battery devices because of the low interfacial resistance, good transport properties, and outstanding ability toward formation of a stable solid-electrolyte-interphase (SEI) layer.[42−45]

With these premises, we hereby present a comprehensive study of the P2-type layered $Na_{0.84}Li_{0.1}Ni_{0.27}Mn_{0.63}O_2$ (namely, NLNMO) successfully prepared via the solid-state reaction method. The resulting oxide is fully characterized from the physicochemical point of view and employed as active material to prepare NIB positive electrodes, which are tested in combination with standard electrolyte and different RTIL-based formulations. Structural and electronic features upon desodiation are dissected from first-principles calculations: charge compensation is mainly ensured by $Ni^{2+}/Ni^{3+}/Ni^{4+}$ redox species, while Mn^{4+} and Li^+ sublattices determine the structural integrity of the lattice with a reduced Jahn−Teller distortion upon Na removal. The NLNMO-based electrodes exhibit enhanced performance in combination with RTIL-based electrolytes, showing superior stability compared to carbonate-based electrodes, along with good structural retention upon cycling. All in all, these findings highlight promising prospects of the investigated setup for future applications in high energy density NIBs.

2. EXPERIMENTAL SECTION

2.1. Synthesis and Characterization Techniques. NLNMO was prepared by a solid-state method. Stoichiometric amounts of sodium carbonate (Na_2CO_3, ≥99.5%, Sigma-Aldrich), lithium carbonate (Li_2CO_3, ≥99%, Sigma-Aldrich), nickel acetate tetrahydrate ($Ni(OCOCH_3)_2·4H_2O$, 98%, Sigma-Aldrich), and manganese acetate tetrahydrate (($CH_3COO)_2Mn·4H_2O$, 99%, Carlo Erba) were premixed and dissolved in a solution of 5% vol. acetic acid and deionized water. The solution was then dried at 80 °C with stirring until drying. The dried precursors were then calcined at 600 °C for 5 h, ground uniformly in an agate mortar, and uniaxially pressed to form green pellets. The final active material powder was obtained by sintering the pellets at 900 °C for 8 h in air followed by grinding in an agate mortar. X-ray diffraction (XRD) was performed by a Panalytical's X'Pert3MRD PRO diffractometer, equipped with a CuKα X-ray source ($V = 40$ kV, $i = 30$ mA) and a curved graphite secondary monochromator. The diffraction profiles were collected directly on the electrodes in the 2θ range between 30° and 70° after peak evaluation in the whole range from 10° to 80°. The morphology of the synthesized powder was analyzed by means of scanning electron microscopy (SEM) with field emission gun (FEG)-SEM (ZEISS Gemini LEO 1530, Germany).

2.2. Computational Details. Spin-polarized density functional theory (DFT) calculations were performed with the DFT + U Hubbard-like correction scheme to overcome the large self-interaction error (SIE) that affects DFT when applied to mid-to-late first-row TM oxides with tightly localized d-electrons.[46−48] Projector-augmented wave (PAW) potentials and plane wave (PW) basis sets were used, as implemented in the Vienna Ab-initio Simulation Package (VASP) code (version 5.4.4).[49] For all of the calculations, the following PAW potentials were considered: Na_pv [Be]2p^{6}3s^1; Li [He]2s^1; Mn
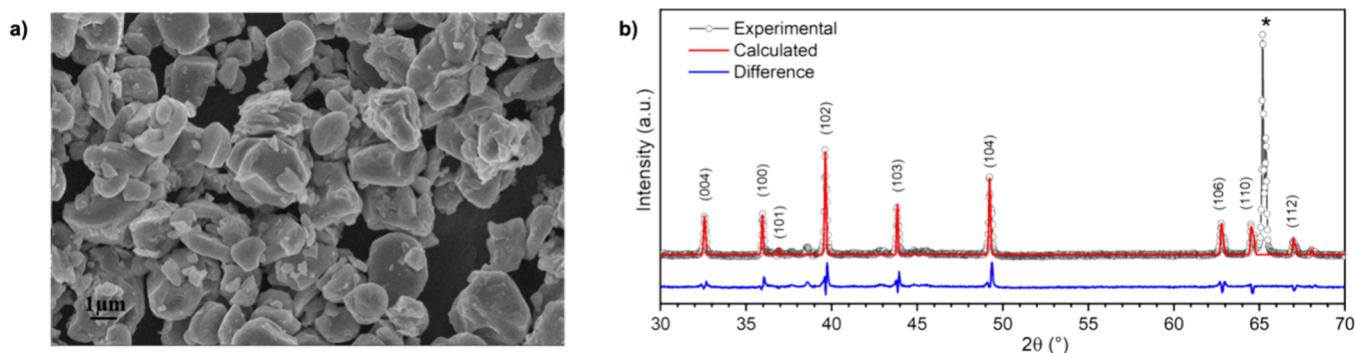
Figure 1. (a) SEM image of the as-synthesized NLNMO powder; (b) Rietveld refinement of the XRD pattern of NLNMO (the intense peak at 65° labeled with the asterisk is due to the underlying Al current collector). The starting structure for the refinement was taken from ref 19. (reproduced from [Xu et al., *Chem. Mater.* **26** (2014) 1260−1269], copyright 2014 American Chemical Society).

[Ar]3d^7; Ni [Ar]3d^{10}; O [He]2s^{2}2p^4.[50,51] The Perdew−Burke−Ernzerhof (PBE) exchange-correlation functional with U_{eff} = 4.0 eV parameter was adopted for both Ni and Mn atoms, and the D3-BJ dispersion correction was added to account for van der Waals (vdW) interactions that play a crucial role in layered structures.[52−54] The PW kinetic energy value and k-points sampling mesh were determined from preliminary convergence tests. For all the calculations, the convergence threshold for energy has been set to 10^{-5} eV. The structural model for Na$_{0.75}$Li$_{0.125}$Ni$_{0.25}$Mn$_{0.625}$O$_2$ consists of a 120 atoms-containing 4 × 4 × 1 supercell of α-NaMnO$_2$ within the $P6_3/mmc$ space group, deriving from the 2 f.u.-containing unit cell of NaMnO$_2$, which allows to model the desired compositions both at the metal and Na sites (i.e., 1:2:5 Li:Ni:Mn and 1:3 vacancy:Na ratios, respectively). The mixed occupancy of Li/Ni/Mn at the corresponding atomic sites results in TM disorder,[7,55] which can be simulated via the special quasi random structure (SQS) approach, as implemented in the Alloy Theoretic Automated Toolkit (ATAT) code.[56−58] Na atoms were placed in edge and face sites with Na(e)/Na(f) ratio being equal to 2.[59] Lattice constants and atomic positions for each Na composition (x_{Na} = 0.75, 0.50, and 0.375) were fully relaxed until the maximum forces acting on each atom were below 0.03 eV/Å. The net magnetic moment on each atom was obtained as the difference in the up and down spin channels integrated within a sphere with a Wigner−Seitz radius for each atom type (default values from VASP are used).

2.3. Electrochemical Measurements. The different RTILs (>99.9 wt %, moisture content <5 ppm), including 1-ethyl-3-methyl-imidazolium bis(fluorosulfonyl)imide (EMI-FSI), 1-butyl-1-methylpyrrolidinium bis(fluorosulfonyl)imide (PYR$_{14}$-FSI), and *N*-trimethyl-*N*-butyl-ammonium bis(fluorosulfonyl)imide (N$_{1114}$-FSI), and the sodium salts (>99.9 wt %, moisture content <5 ppm), including sodium bis(fluorosulfonyl)imide (NaFSI) and sodium perchlorate (NaClO$_4$), were provided by Solvionic (France) and used as received. Propylene carbonate (PC, anhydrous, 99.7%) was provided by Merck and stored in a controlled Ar-atmosphere dry glovebox (MBraun UNILab, H$_2$O and O$_2$ content <1 ppm) with molecular sieves. The RTIL-based and standard electrolyte formulations were prepared in the glovebox: proper amounts of the selected sodium salt were dissolved in each RTIL by stirring at ambient temperature for few hours. The RTIL:sodium salt molar ratio was fixed to 4:1,[42,60] while the standard electrolyte was prepared by dissolving NaClO$_4$ in PC (1M). Positive electrodes were prepared with the following composition: 80 wt % of active material Na$_{0.84}$Li$_{0.1}$Ni$_{0.27}$Mn$_{0.63}$O$_2$, 10 wt % of electrically conductive agent (carbon black CNERGY Super C65), and 10 wt % of poly(vinylidene difluoride) PVdF (Solvay Solef 2010) as a binder. First, powders of active material and C65 were gently mixed in a hand mortar. Successively, the mixture was added to a solution of PVdF in *N*-methyl pyrrolidone (NMP, Merck) under constant stirring, which was continued for ~3−4h at ambient laboratory temperature (i.e., ~ 21 °C). The resulting dense and homogeneous slurry was casted onto an Al current collector using a doctor blade. The NMP solvent was removed by evaporation at ambient temperature, and the electrodes

were further dried at 120 °C/vacuum for 24 h prior to utilization. The materials were tested in laboratory-scale Na-metal cells (ECC-Std test cells by EL-Cell Gmbh), which were assembled by sandwiching sodium metal anode and NLNMO cathode disks having an area of 2.54 cm^2 (mass loading of 2.30 ± 0.15 mg cm^{-2}) in a Na/electrolyte/NLNMO configuration. The Na-metal cells for the cyclic voltammetry (CV) measurement were assembled with a cathode loading of 1.5 mg cm^{-2}. Glass fiber (Whatman GF/A) 100 μm-thick disks (2.54 cm^2 area) were used as separators with 250 μL of selected electrolyte uptake. The laboratory-scale cells were assembled inside the dry glovebox and tested under constant current (galvanostatic) regime in a range of voltage between 2.1 and 4.0 V vs Na$^+$/Na at ambient laboratory temperature using an Arbin BT2000 battery tester.

3. RESULTS AND DISCUSSION

Synthesis of NLNMO via the solid-state reaction method leads to uniform powders, showing a homogeneous particle size distribution in the range from 1 to 3 μm (see Figure 1a). XRD analysis together with Rietveld refinement confirms the distinctive P2-type structure with the $P6_3/mmc$ space group and lattice parameters a = 2.8838 Å and c = 11.0046 Å comparable to the literature (i.e., a = 2.8852 Å and c = 11.0162 Å, Figure 1b).[19] The larger deviation is found on the c-axis, which seems slightly compressed (see Table S1 in the Supporting Information).

XRD results can be directly compared to theoretical insights gained by DFT calculations. NLNMO has been modeled as Na$_{0.75}$Li$_{0.125}$Ni$_{0.25}$Mn$_{0.625}$O$_2$ stoichiometry, which complies with the nominal experimental composition. Being aware of the influence on relevant properties, we take structural disorder into account in our theoretical model. On the one hand, we enclose a random distribution of Li:Ni:Mn at the metal site for a highly disordered model that would reflect the isotropic properties and align with the absence of local aggregation in real samples.[7,55] On the other hand, we entail a Na$^+$/vacancy ordering that mirrors the 2:1 Na(face):Na(edge) ratio as previously reported,[59] which is rather kept constant upon desodiation of Na$_x$Li$_{0.125}$Ni$_{0.25}$Mn$_{0.75}$O$_2$. While the Na$^+$ displacement from less stable face sites toward edge and pseudo-octahedral positions has been addressed as a thermodynamic driving force in the P2-OP4 phase transition upon Na$_x$MnO$_2$ charging,[61] the constant ratio obtained for Na$_x$Li$_{0.125}$Ni$_{0.25}$Mn$_{0.75}$O$_2$ would suggest a hindered Na displacement and, thus, a high P2 structure retention upon desodiation. The minimum-energy structure obtained at the PBE + U(-D3BJ) level of theory shows good agreement with the XRD results (Table S2 in the Supporting Information). To
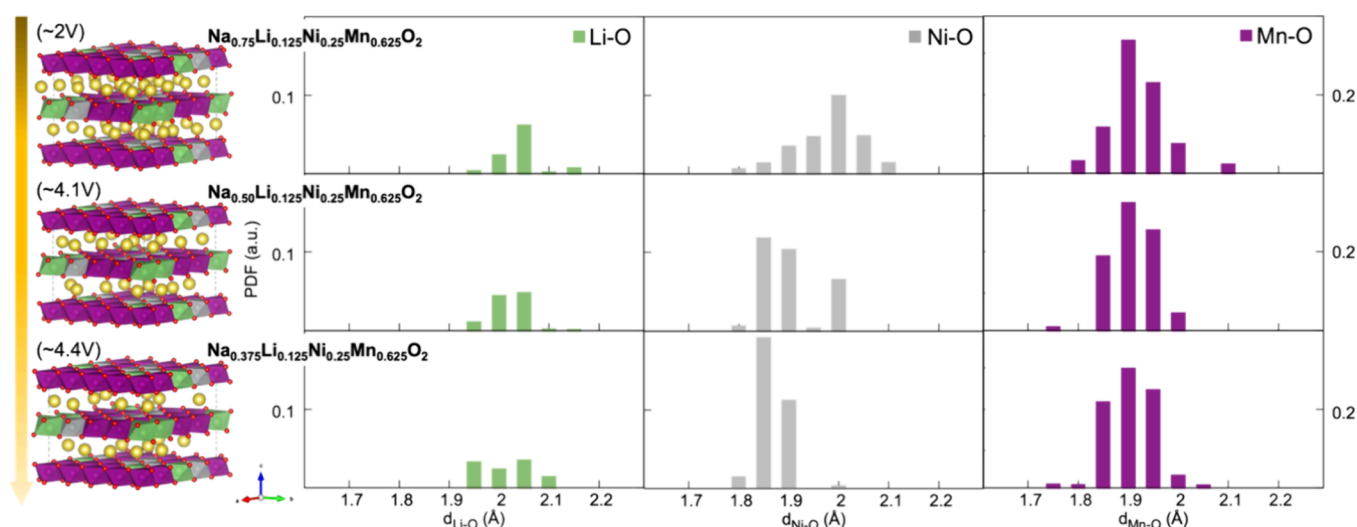
Figure 2. Pair distribution functions of Li−O (green), Ni−O (gray), and Mn−O (purple) distances in $Na_{0.75}Li_{0.125}Ni_{0.25}Mn_{0.625}O_2$ calculated at the PBE + U(-D3BJ) level of theory at different Na contents. Structural models are displayed on the left-hand side to associate the corresponding state of charge. Color code: Na (yellow), Li (green), Ni (gray), Mn (purple), and O (red). Atoms are depicted as spheres, and MO_6 octahedra are highlighted as polyhedrons.
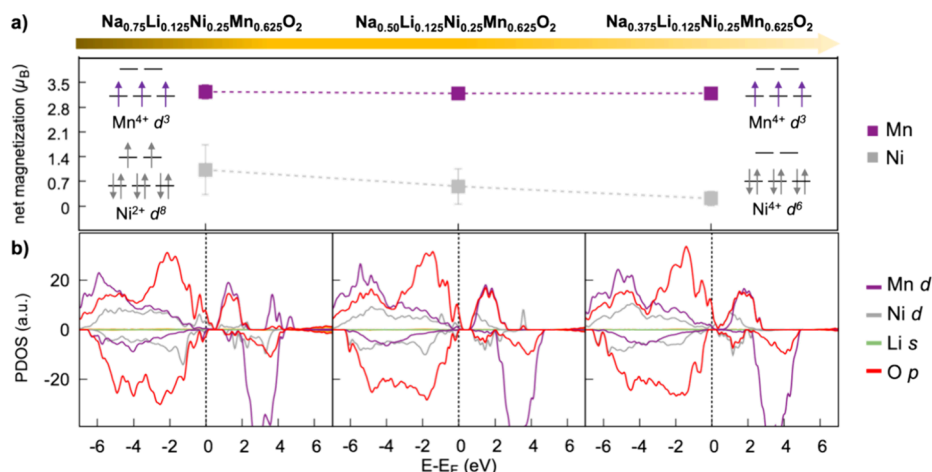

Figure 3. Electronic structure analysis of NLNMO as a function of Na content performed at the PBE + U(-D3BJ) level of theory: (a) net magnetization averaged on Mn and Ni sublattices; (b) atom- and angular momentum-projected density of states (PDOS). The color code is declared on the right side.

dissect the role of each metal dopant and understand the cathode electrochemical behavior, we have simulated the desodiation process occurring upon charge by varying the Na content within the parent structures ($Na_{0.75}Li_{0.125}Ni_{0.25}Mn_{0.625}O_2$, $Na_{0.50}Li_{0.125}Ni_{0.25}Mn_{0.625}O_2$, and $Na_{0.375}Li_{0.125}Ni_{0.25}Mn_{0.625}O_2$, as displayed on the left side of Figure 2). The selected sodiation contents used in the DFT simulations can be directly correlated to the states of charge adopted by the cathode upon cycling. As shown later in the text, even though the electrochemical measurements are not run above 4.1 V, the lowest sodium content ($x_{Na} = 0.375$) is still required as a theoretical reference of the upper desodiation limit. Indeed, the sodium intercalation potential can be calculated from first principles according to the following equation:

$$V = \frac{E_{Na_{x_2}LNMO} - E_{Na_{x_1}LNMO} - (x_2 - x_1)\frac{1}{2}E_{Na}}{(x_2 - x_1)} \quad (1)$$

where $E_{Na_{x_2}LNMO}$ and $E_{Na_{x_1}LNMO}$ are the total energies of the NLNMO cathode material at, respectively, x_2 and x_1 sodium contents ($x_2 > x_1$), and E_{Na} is the total energy of sodium metal in its 2-atoms containing a bcc lattice used as a reference. This represents a well-established method to predict the cathode behavior upon charge.[36−38,62] Analysis of pair distribution functions (PDFs) as a function of sodium content can unveil the possible structural transformations occurring within MO_6 octahedra upon desodiation (see Figure 2). While Li−O and Mn−O distances are retained upon Na extraction, the Ni−O ones clearly undergo bond shortening at decreasing Na content. As already reported in previous studies, the left-shifting trend of the short-range distances suggests a general compression of the MO_6 octahedra as a result of the underlying metal oxidation.[36−38]

Electronic structure calculations can unveil the redox-active mechanisms for charge compensation. The magnetization trends upon desodiation reveal that the Mn^{4+} oxidation state is clearly retained (see purple lines in Figure 3a), while the Ni
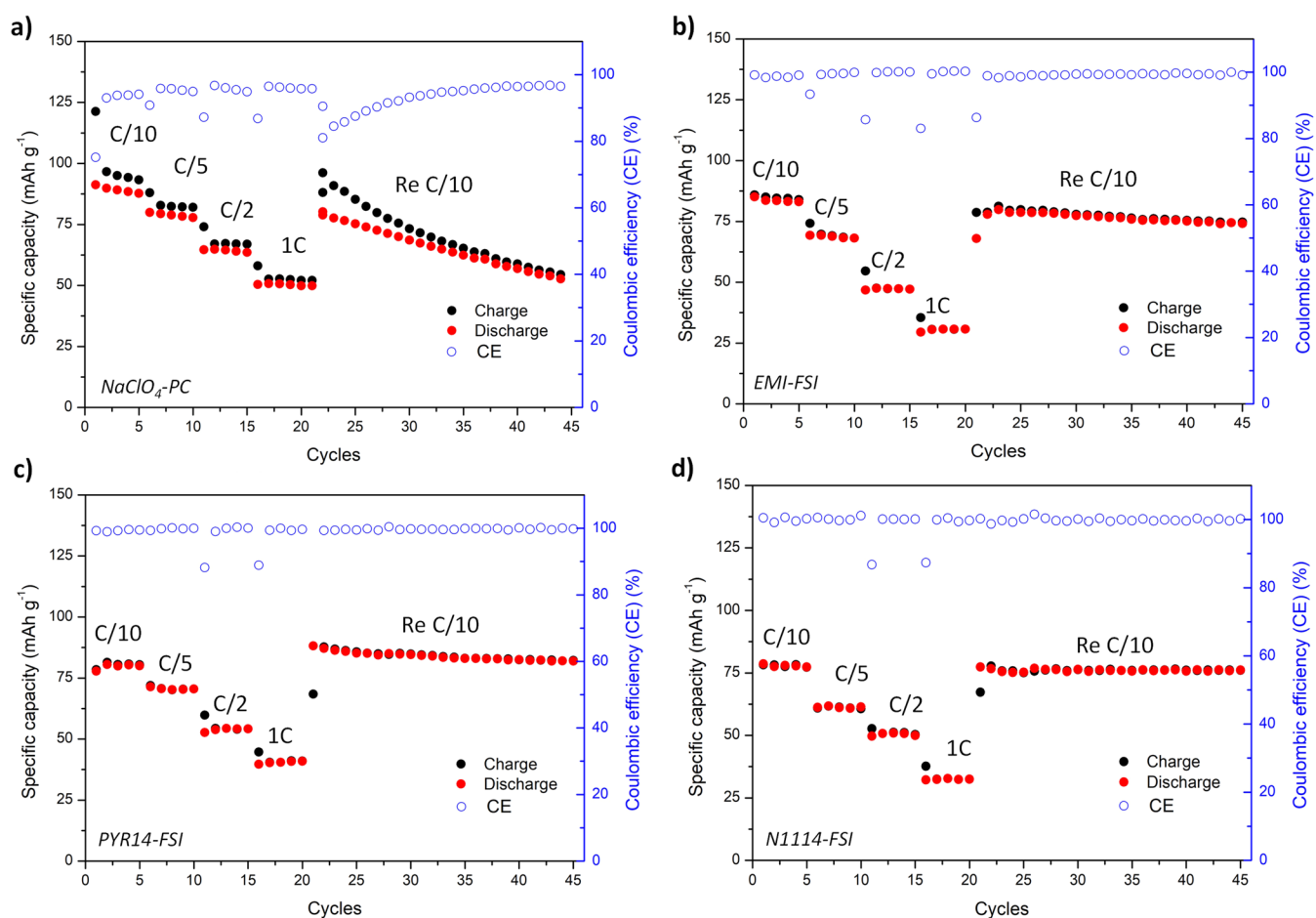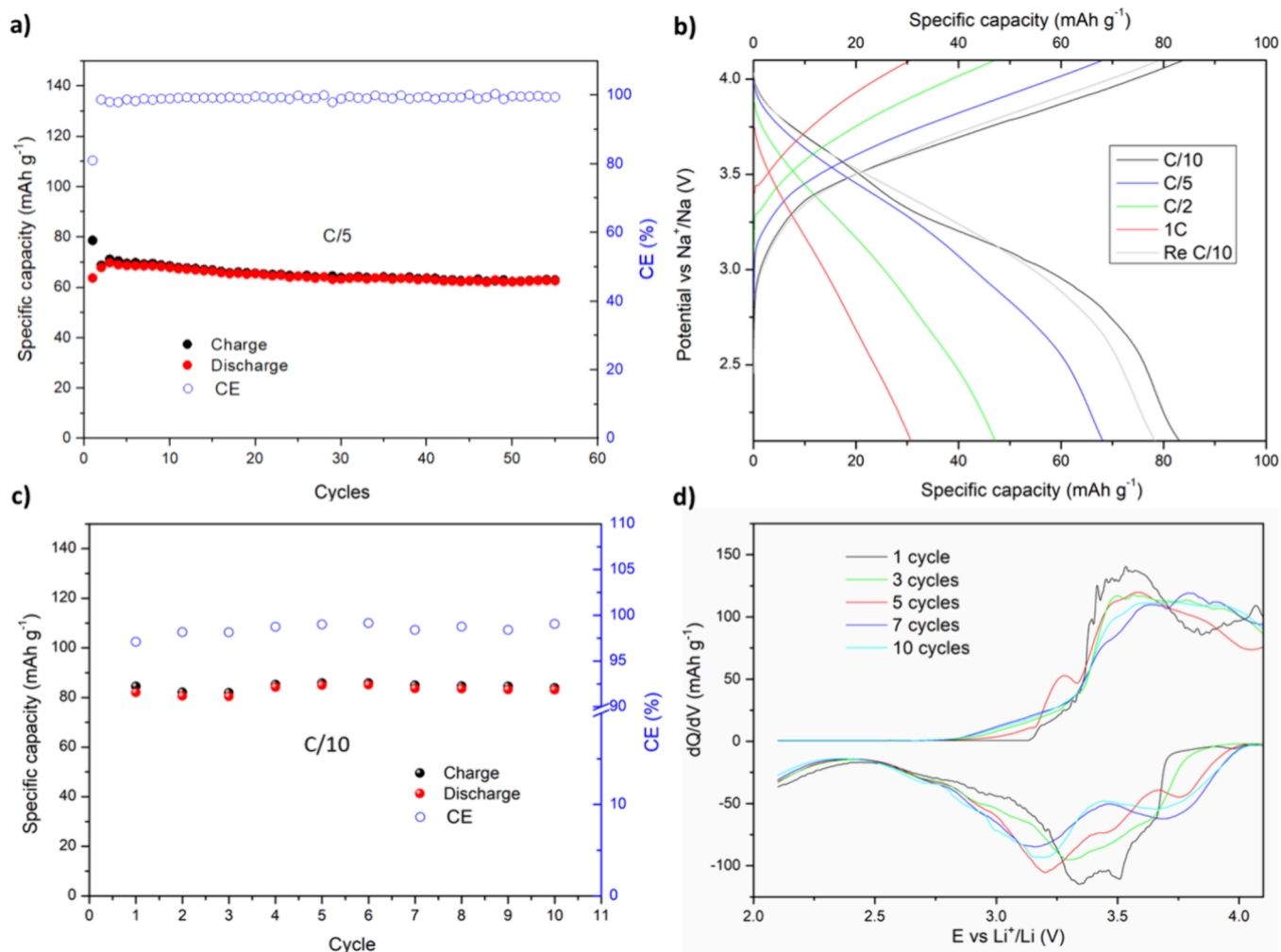
Figure 4. Specific capacity vs cycles plots of Na-metal cells assembled with NLNMO and (a) standard NaClO$_4$/PC liquid electrolyte; (b−d) three RTIL-based electrolytes galvanostatically cycled at different current regimes (C/10, C/5, C/2, and 1C) under ambient laboratory temperature.

sublattice plays the redox active role and compensates for the Na$^+$ removal by undergoing Ni^{2+} → Ni^{3+} → Ni^{4+} oxidation (see gray lines in Figure 3a). Further calculations performed at different U_{eff} values on the Mn d shell endorse the constant trend of magnetization values on Mn sites along desodiation, as reported in Table S3. While confirming the previous discussion from PDF analysis on the different electrochemical role exerted by the TM sublattices, the electronic structure analysis can provide further insights on the charge compensation mechanisms that are activated in the NLNMO cathode upon charge. Noteworthily, the atom- and angular momentum-projected density of states (PDOS, Figure 3b) shows the O p state band crossing the Fermi level, leading to p-type conductivity burdened by the formation of electron holes on oxygen atoms. Evidence of any triggerable oxygen redox process highlights a non-innocent role in participating to charge compensation, which is usually featured in similar layered transition metal oxide cathodes in the high operating voltage range. Our findings are in close agreement to recent DFT and XAS results by Zhao et al. for the closely related Na$_{10−x}$LiNi$_3$Mn$_8$O$_{24}$-layered oxide, which indicate electron extraction taking place from Ni 3d states upon charge and O 2p states starting to participate at high desodiation degrees.[21]

The electrochemical compatibility and stability of the novel NLNMO composition have been evaluated in combination with different electrolytes through galvanostatic cycling at ambient laboratory temperature (~21 °C) and at different

increasing current regimes (C-rates of C/10, C/5, C/2, and 1C) calculated from the theoretical specific capacity of the active electrode material that can desodiate in the explored voltage range up to x_{Na} = 0.375, i.e., 102 mAh g^{-1} (namely, the practical theoretical specific capacity, obtained by considering a molecular weight of 98.6 g mol^{-1} for Na$_{0.84}$Li$_{0.1}$Ni$_{0.27}$Mn$_{0.63}$O$_2$ and an electric charge exchange of 0.375·96500 C per mol of cathode compound). The voltage range has been defined after CV test performed with a standard liquid electrolyte (see Figure S1 in the Supporting Information), which allowed to detect a reversible redox activity within the 2.1−4.0 V vs Na$^+$/Na range.[63] During the first two cycles, the two peaks observed between 2.5 and 3.7 V do not decrease significantly in intensity, indicating good initial reversibility. As shown in Figure 4a, the NLNMO electrode in combination with conventional NaClO$_4$/PC electrolyte delivers a specific capacity of ~90 mAh g^{-1} at C/10, which decreases to 50 mAh g^{-1} at 1C rate. The specific capacity of NLNMO is in line with the results reported in the recent literature about P2-type layered oxides as NIB cathode materials, briefly summarized in Table S4.[10,64] Indeed, after the C-rate test with increasing current rate from C/10 to 1C, the prolonged cycling at C/10 evidences a gradual, significant decrease in specific capacity values with time/cycles, i.e., down to 50 mAh g^{-1} after only 45 cycles (viz., below 50% of the above-reported practical theoretical specific capacity of the material). This trend suggests a poor compatibility of this specific layered oxide

Figure 5. Electrochemical behavior of the laboratory-scale Na-metal cell assembled with the EMI-FSI-based electrolyte: (a) plot of specific capacity vs cycles at C/5; (b) plot of charge/discharge profiles vs specific capacity at different C rates; (c) plot of specific capacity vs cycles at C/10; (d) related dQ/dV profiles extrapolated at different cycles.

cathode structure with the standard electrolyte and the formation of a poor passivation layer, which is not preventing the solubilization of TM ions in the electrolyte and the following collapse of the layered structure upon cycling. Proper selection of the electrolyte can inhibit such decay in electrochemical performance, specifically by enhancing the quality of the passivation layer obtained over the cathode at high anodic potential and thus mitigating the structural degradation of the electrode active material particles. In this context, RTIL-based electrolytes are considered extremely promising to guarantee improved performances.[65,66] The laboratory-scale cells prepared using different RTIL-based electrolytes (Figure 4b−d) show a similar behavior at C/10, delivering only a slightly lower initial specific capacity compared to that of the $NaClO_4$/PC liquid electrolyte (Figure 4a). During initial charge/discharge at C/10, higher values are obtained with the EMI-FSI electrolyte, which allows to achieve 86 mAh g^{-1} (Figure 4b); meanwhile, PYR$_{14}$-FSI and N$_{1114}$-FSI approach 80 mAh g^{-1} (Figure 4c,d). Interestingly, the specific capacity gained by the $NaClO_4$/PC electrolyte approaches 88% of the calculated practical theoretical capacity, while the RTIL-based cells turn out to approach ∼85% of the maximum capacity achievable under C/10 and ambient laboratory temperature conditions. Nevertheless, it is worth to notice

that the RTIL-based cells are not at all affected by the gradual decrease in specific capacity upon time/cycling, and the capacity retention percentages after more than 45 cycles are 90, 98, and 97% for EMI-, PYR$_{14}$-, and N$_{1114}$-FSI-based cells, respectively, in contrast with the low residual capacity delivered by the conventional liquid electrolyte-based cell. The different electrochemical behavior observed for these electrolytes can be explained by tracing back to fundamental physical-chemical properties. Organic solvent-based electrolytes, i.e., carbonates (EC and PC), are usually known to exhibit higher ionic conductivities than RTILs, which can be ascribed to the much lower viscosity values (e.g., at 25 °C, the viscosity is 2.5 mPa s for PC, while for RTILs, it ranges from 24.5 mPa s for EMI-FSI to 64.1 mPa s for Pyr$_{14}$-FSI). According to the Walden law, the viscosity−conductivity inverse dependency would also rationalize the better electrochemical performances observed with the less viscous and, thus, more conductive EMIFSI-based electrolyte. Still, the low-volatile RTILs usually come with a wider thermal and electrochemical stability range compared to the more volatile organic solvents, which could explain the higher capacity retention in RTIL-based cells. These results clearly state the enhanced compatibility of the NLNMO cathode under study with RTIL-based electrolyte solutions, which allow for much

more stable cycling even at higher Coulombic efficiency (CE) both at low and high C-rates. Indeed, the CE of the RTIL-based cells approaches 100% during the whole cycling test, while the CE of the standard electrolyte cell never increases above 96%.

Considering the preliminary results at C/10 rate and the similar behavior in terms of specific capacity output and CE obtained with RTIL-based electrolytes, EMI-FSI has been chosen as a representative sample for further characterization because of its lower viscosity and, in turn, higher conductivity, as well as lower cost, which is important in view of future scale-up based on the envisaged application. A preliminary long-term stability test has also been performed over 55 cycles at C/5, as shown in Figure 5a. We have selected the last cycles of each C-rate step of the EMI-FSI-based cell (i.e., 5th, 10th, 15th, 20th, and 25th) to plot the charge/discharge voltage profile vs specific capacity (Figure 5b). Slight changes in voltage profiles are observed as a result of the increasing C-rate, meaning that at higher C-rate, the impedance contribution increases and the higher polarization causes the appearance of sloppy profiles rather than the well-defined plateaus, typically accounting for characteristic material redox reactions. Nevertheless, the voltage plot highlights the good capacity retention at ReC/10 after the test at relatively high C-rates. At the same time, the minor change in the profile shape at ReC/10 could be associated with little electrode structural variation.[67] Differential capacity analysis (dQ/dV) has been applied to data collected on a fresh EMI-FSI-based cell at a slow rate (C/10) to better resolve the electrode features and to minimize the impedance effects on the profiles (Figure 5c,d). The features of the dQ/dV plot in Figure 5d are assigned to the oxide electrode, and they are correlated to the CV analysis (Figure S1 in the Supporting Information). Notably, the minor modification in the peak profile along with cycling can be ascribed to small structural rearrangements, especially upon discharge where two defined peaks arise after few cycles.

To assess whether prolonged cycling affects the structural stability of the electrode, XRD analysis was performed after 10 cycles at C/10 (Figure S2 in the Supporting Information). The spectra after cycling exhibits alterations compared to that of the fresh electrode. Both broadening and the intensity decrease of the distinctive peaks of the P2-type structure are most likely due to distortion across the entire structure associated with a decrease in crystallinity and uneven spacing between layers; anyhow, it is important to remark that these minor inconsistencies apparently do not compromise the structure, as also suggested by our computational models.[67] The P2 phase acts as a support, alleviating the structural strain associated with the transition between composite phases P2-P2/O3-P3 during the desodiation process. The minor structural rearrangement confirms the relatively high stability and compatibility of the NLNMO electrode in combination with RTIL-based electrolytes without using any further additive (e.g., PC, FEC, VC, etc.), which is conversely typically done to stabilize the cathode/electrode interface and the layered oxide structure upon prolonged cycling.[68]

4. CONCLUSIONS

Here, we have studied and developed a P2-type layered Li-doped Na_xTMO_2 oxide as a high-energy cathode for Na-ion batteries. The NLNMO composition has been synthesized via the solid-state method, structurally and morphologically characterized by XRD and SEM analyses and DFT

calculations, and then ultimately tested as an active cathode material in combination with RTIL-based electrolyte formulations. The main outcomes of this thorough material investigation can be summed up as follows:

- The structural features of the synthesized P2 phase are retained upon prolonged cycling, as confirmed by the minor changes in the XRD spectra recorded after cycling. Through synergistic action, the composite phases P2-P2/O3-P3 collaborate to alleviate the structural strain, reduce the lattice mismatch, and prevent the sliding of the TM plate. DFT calculations reveal that the structural integrity of the lattice is ensured by Mn^{4+} and Li^+ sublattices, with a reduced Jahn−Teller distortion upon Na removal.

- The good redox reversibility attested by CV measurements is unveiled from first principles as mainly associated with $Ni^{2+} \rightarrow Ni^{3+} \rightarrow Ni^{4+}$, exerting the redox active role and burdening the charge compensation upon sodiation/desodiation.

- Although the specific capacity delivered by the NLNMO cathode in combination with the conventional $NaClO_4$/PC liquid electrolyte is slightly higher (90 mAh g^{-1} vs 86−80 mAh g^{-1} for $NaClO_4$/PC and NaFSI/RTILs, respectively), electrochemical performance with all the three (i.e., NaFSI/EMI-FSI, PYR_{14}-FSI, and N_{1114}-FSI) RTIL-based formulations is enhanced in terms of reversible cycling stability and specific capacity retention over prolonged cycling (i.e., 90, 98, and 97% vs 60% for NaFSI/EMI-FSI, NaFSI/PYR_{14}-FSI, and NaFSI/N_{1114}-FSI vs $NaClO_4$/PC, respectively).

As a result, the P2-type NLNMO-based electrode exhibits promising electrochemical behavior in combination with RTILs, which paves the route toward its application in future high energy density NIB devices.

■ ASSOCIATED CONTENT

Ⓢ Supporting Information

The Supporting Information is available free of charge at https://pubs.acs.org/doi/10.1021/acs.chemmater.4c01311.

> Rietveld refinement results; lattice constants calculated from DFT results; magnetic moments obtained with different U_{eff} values; CV profile with the $NaClO_4$/PC electrolyte; XRD profile of pristine and cycled electrodes (PDF)

■ AUTHOR INFORMATION

Corresponding Authors

Michele Pavone − *Department of Chemical Sciences, University of Naples Federico II, Napoli 80126, Italy; National Reference Centre for Electrochemical Energy Storage (GISEL), INSTM, Firenze 50121, Italy;* ⓘ orcid.org/0000-0001-7549-631X; Email: michele.pavone@unina.it

Claudio Gerbaldi − *GAME Lab, Department of Applied Science and Technology (DISAT), Politecnico di Torino, Torino 10129, Italy; National Reference Centre for Electrochemical Energy Storage (GISEL), INSTM, Firenze 50121, Italy;* ⓘ orcid.org/0000-0002-8084-0143; Email: claudio.gerbaldi@polito.it

Authors

Arianna Massaro − *Department of Chemical Sciences, University of Naples Federico II, Napoli 80126, Italy;*

National Reference Centre for Electrochemical Energy Storage (GISEL), INSTM, Firenze 50121, Italy; ● orcid.org/0000-0003-2950-6745

Gabriele Lingua − *National Reference Centre for Electrochemical Energy Storage (GISEL), INSTM, Firenze 50121, Italy; GAME Lab, Department of Applied Science and Technology (DISAT), Politecnico di Torino, Torino 10129, Italy; Present Address: POLYMAT, University of the Basque Country UPV/EHU, Avenida Tolosa 72, Gipuzkoa, 20018 Donostia-San Sebastian, Spain (G.L.)*

Francesco Bozza − *Energy Technologies and Renewable Sources Department (ENEA), Roma 00123, Italy*

Alessandro Piovano − *GAME Lab, Department of Applied Science and Technology (DISAT), Politecnico di Torino, Torino 10129, Italy; National Reference Centre for Electrochemical Energy Storage (GISEL), INSTM, Firenze 50121, Italy;* ● orcid.org/0000-0002-5784-6897

Pier Paolo Prosini − *Energy Technologies and Renewable Sources Department (ENEA), Roma 00123, Italy*

Ana B. Muñoz-García − *National Reference Centre for Electrochemical Energy Storage (GISEL), INSTM, Firenze 50121, Italy; Department of Physics "E. Pancini", University of Naples Federico II, Napoli 80126, Italy;* ● orcid.org/0000-0002-9940-7358

Complete contact information is available at:
https://pubs.acs.org/10.1021/acs.chemmater.4c01311

Notes

The authors declare no competing financial interest.

■ **REFERENCES**

(1) Ferrari, S.; Falco, M.; Muñoz-García, A. B.; Bonomo, M.; Brutti, S.; Pavone, M.; Gerbaldi, C. Solid-State Post Li Metal Ion Batteries: A Sustainable Forthcoming Reality? *Adv. Energy Mater.* **2021**, *11* (43), No. 2100785.

(2) Kubota, K.; Komaba, S. Review—Practical Issues and Future Perspective for Na-Ion Batteries. *J. Electrochem. Soc.* **2015**, *162* (14), A2538−A2550.

(3) Nayak, P. K.; Yang, L.; Brehm, W.; Adelhelm, P. From Lithium-Ion to Sodium-Ion Batteries: Advantages, Challenges, and Surprises. *Angew. Chemie Int. Ed.* **2018**, *57* (1), 102−120.

(4) Chayambuka, K.; Mulder, G.; Danilov, D. L.; Notten, P. H. L. Sodium-Ion Battery Materials and Electrochemical Properties Reviewed. *Adv. Energy Mater.* **2018**, *8* (16), No. 1800079.

(5) Karabelli, D.; Singh, S.; Kiemel, S.; Koller, J.; Konarov, A.; Stubhan, F.; Miehe, R.; Weeber, M.; Bakenov, Z.; Birke, K. P. Sodium-Based Batteries: In Search of the Best Compromise Between Sustainability and Maximization of Electric Performance. *Front. Energy Res.* **2020**, *8*, No. 605129.

(6) Liu, Q.; Hu, Z.; Chen, M.; Zou, C.; Jin, H.; Wang, S.; Chou, S.-L.; Dou, S.-X. Recent Progress of Layered Transition Metal Oxide Cathodes for Sodium-Ion Batteries. *Small* **2019**, *15* (32), No. 1805381.

(7) Zhang, Y.; Zhang, R.; Huang, Y. Air-Stable Na$_x$TMO$_2$ Cathodes for Sodium Storage. *Front. Chem.* **2019**, *7*, 335.

(8) Brugnetti, G.; Triolo, C.; Massaro, A.; Ostroman, I.; Pianta, N.; Ferrara, C.; Sheptyakov, D.; Muñoz-García, A. B.; Pavone, M.; Santangelo, S.; Ruffo, R. Structural Evolution of Air-Exposed Layered Oxide Cathodes for Sodium-Ion Batteries: An Example of Ni-Doped Na$_x$ MnO$_2$. *Chem. Mater.* **2023**, *35* (20), 8440−8454.

(9) Massaro, A.; Fasulo, F.; Pecoraro, A.; Langella, A.; Muñoz-García, A. B.; Pavone, M. First-Principles Design of Nanostructured Electrode Materials for Na-Ion Batteries: Challenges and Perspectives. *Phys. Chem. Chem. Phys.* **2023**, *25* (28), 18623−18641.

(10) Zuo, W.; Innocenti, A.; Zarrabeitia, M.; Bresser, D.; Yang, Y.; Passerini, S. Layered Oxide Cathodes for Sodium-Ion Batteries: Storage Mechanism, Electrochemistry, and Techno-Economics. *Acc. Chem. Res.* **2023**, *56* (3), 284−296.

(11) Luo, K.; Roberts, M. R.; Hao, R.; Guerrini, N.; Pickup, D. M.; Liu, Y. S.; Edström, K.; Guo, J.; Chadwick, A. V.; Duda, L. C.; Bruce, P. G. Charge-Compensation in 3d-Transition-Metal-Oxide Intercala-tion Cathodes through the Generation of Localized Electron Holes on Oxygen. *Nat. Chem.* **2016**, *8* (7), 684−691.

(12) House, R. A.; Maitra, U.; Pérez-Osorio, M. A.; Lozano, J. G.; Jin, L.; Somerville, J. W.; Duda, L. C.; Nag, A.; Walters, A.; Zhou, K. J.; Roberts, M. R.; Bruce, P. G. Superstructure Control of First-Cycle Voltage Hysteresis in Oxygen-Redox Cathodes. *Nature* **2020**, *577* (7791), 502−508.

(13) Zhao, C.; Wang, Q.; Yao, Z.; Wang, J.; Sánchez-Lengeling, B.; Ding, F.; Qi, X.; Lu, Y.; Bai, X.; Li, B.; Li, H.; Aspuru-Guzik, A.; Huang, X.; Delmas, C.; Wagemaker, M.; Chen, L.; Hu, Y.-S. Rational Design of Layered Oxide Materials for Sodium-Ion Batteries. *Science (80-.).* **2020**, *370* (6517), 708−711.

(14) Ma, C.; Alvarado, J.; Xu, J.; Clément, R. J.; Kodur, M.; Tong, W.; Grey, C. P.; Meng, Y. S. Exploring Oxygen Activity in the High Energy P2-Type Na$_{0.78}$Ni$_{0.23}$Mn$_{0.69}$O$_2$ Cathode Material for Na-Ion Batteries. *J. Am. Chem. Soc.* **2017**, *139* (13), 4835−4845.

(15) Bella, F.; Muñoz-García, A. B.; Colò, F.; Meligrana, G.; Lamberti, A.; Destro, M.; Pavone, M.; Gerbaldi, C. Combined Structural, Chemometric, and Electrochemical Investigation of Vertically Aligned TiO$_2$ Nanotubes for Na-Ion Batteries. *ACS Omega* **2018**, *3* (7), 8440−8450.

(16) Hou, D.; Gabriel, E.; Graff, K.; Li, T.; Ren, Y.; Wang, Z.; Liu, Y.; Xiong, H. Thermal Dynamics of P2-Na0.67Ni0.33Mn0.67O2 Cathode Materials for Sodium Ion Batteries Studied by in Situ Analysis. *J. Mater. Res.* **2022**, *37* (6), 1156−1163.

(17) Risthaus, T.; Zhou, D.; Cao, X.; He, X.; Qiu, B.; Wang, J.; Zhang, L.; Liu, Z.; Paillard, E.; Schumacher, G.; Winter, M.; Li, J. A High-Capacity P2 Na$_{2/3}$Ni$_{1/3}$Mn$_{2/3}$O$_2$ Cathode Material for Sodium Ion Batteries with Oxygen Activity. *J. Power Sources* **2018**, *395*, 16−24.

(18) Kim, D.; Kang, S.-H.; Slater, M.; Rood, S.; Vaughey, J. T.; Karan, N.; Balasubramanian, M.; Johnson, C. S. Enabling Sodium Batteries Using Lithium-Substituted Sodium Layered Transition Metal Oxide Cathodes. *Adv. Energy Mater.* **2011**, *1* (3), 333−336.

(19) Xu, J.; Hoe Lee, D.; Clément, R. J.; Yu, X.; Leskes, M.; Pell, A. J.; Pintacuda, G.; Yang, X.-Q.; Grey, C. P.; Shirley Meng, Y.

Identifying the Critical Role of Li Substitution in P2—Na$_x$-[Li$_y$Ni$_z$Mn$_{1-y-z}$]O$_2$ (0 < x, y, z < 1) Intercalation Cathode Materials for High-Energy Na-Ion Batteries. *Chem. Mater.* **2014**, *26* (2), 1260−1269.

(20) Zhao, C.; Li, C.; Yang, Q.; Qiu, Q.; Tong, W.; Zheng, S.; Ma, J.; Shen, M.; Hu, B. Anionic Redox Reaction in Na-Deficient Layered Oxide Cathodes: Role of Sn/Zr Substituents and in-Depth Local Structural Transformation Revealed by Solid-State NMR. *Energy Storage Mater.* **2021**, *39*, 60−69.

(21) Zhao, C.; Yao, Z.; Wang, Q.; Li, H.; Wang, J.; Liu, M.; Ganapathy, S.; Lu, Y.; Cabana, J.; Li, B.; Bai, X.; Aspuru-Guzik, A.; Wagemaker, M.; Chen, L.; Hu, Y.-S. Revealing High Na-Content P2-Type Layered Oxides as Advanced Sodium-Ion Cathodes. *J. Am. Chem. Soc.* **2020**, *142* (12), 5742−5750.

(22) Li, Z.-Y.; Ma, X.; Sun, K.; He, L.; Li, Y.; Chen, D. Na$_2$/3Li$_1$/9[Ni$_2$/9Li$_1$/9Mn$_2$/3]O$_2$: A High-Performance Solid-Solution Reaction Layered Oxide Cathode Material for Sodium-Ion Batteries. *ACS Appl. Energy Mater.* **2022**, *5* (1), 1126−1135.

(23) Liao, Y.; Feng, H.; Yang, Q.; Shen, M.; Jiang, Y.; Li, C.; Zhao, C.; Geng, F.; Hu, B. Oxygen Redox Activation at Initial Cycle to Improve Cycling Stability for the Na$_0.83$Li$_0.12$Ni$_0.22$Mn$_0.66$O$_2$ System. *ACS Appl. Mater. Interfaces* **2023**, *15* (8), 10709−10717.

(24) Saubanère, M.; McCalla, E.; Tarascon, J. M.; Doublet, M. L. The Intriguing Question of Anionic Redox in High-Energy Density Cathodes for Li-Ion Batteries. *Energy Environ. Sci.* **2016**, *9* (3), 984−991.

(25) Vergnet, J.; Saubanère, M.; Doublet, M.-L.; Tarascon, J.-M. The Structural Stability of P2-Layered Na-Based Electrodes during Anionic Redox. *Joule* **2020**, *4* (2), 420−434.

(26) Kim, M.; Kim, H.; Cho, M.; Kim, D. Unlocking Veiled Oxygen Redox in Na-Based Earth-Abundant Binary Layered Oxide. *J. Mater. Chem. A* **2021**, *9* (27), 15179−15187.

(27) Qiu, J.; Chen, B.; Hou, H.; Wang, X.; Liu, X.; Li, Z.; Liu, T.; Chen, R.; Wang, S.; Li, B.; Dai, D.; Wang, B. Improving Na + Diffusion and Performance of P2-Type Layered Na 0.6 Li 0.07 Mn 0.66 Co 0.17 Ni 0.17 O 2 by Expanding the Interplanar Spacing. *ACS Appl. Mater. Interfaces* **2020**, *12* (43), 48669−48676.

(28) Xie, Y.; Gabriel, E.; Fan, L.; Hwang, I.; Li, X.; Zhu, H.; Ren, Y.; Sun, C.; Pipkin, J.; Dustin, M.; Li, M.; Chen, Z.; Lee, E.; Xiong, H. Role of Lithium Doping in P2-Na$_0.67$Ni$_0.33$Mn$_0.67$O$_2$ for Sodium-Ion Batteries. *Chem. Mater.* **2021**, *33* (12), 4445−4455.

(29) Zhao, S.; Jiang, W.; Zhu, X.; Ling, M.; Liang, C. Understanding the Synthesis of Inorganic Solid-State Electrolytes for Li Ion Batteries: Features and Progress. *Sustain. Mater. Technol.* **2022**, *33*, No. e00491.

(30) Islam, M. S.; Fisher, C. A. J. Lithium and Sodium Battery Cathode Materials: Computational Insights into Voltage, Diffusion and Nanostructural Properties. *Chem. Soc. Rev.* **2014**, *43* (1), 185−204.

(31) Morgan, L. M.; Mercer, M. P.; Bhandari, A.; Peng, C.; Islam, M. M.; Yang, H.; Holland, J.; Coles, S. W.; Sharpe, R.; Walsh, A.; Morgan, B. J.; Kramer, D.; Islam, M. S.; Hoster, H. E.; Edge, J. S.; Skylaris, C.-K. Pushing the Boundaries of Lithium Battery Research with Atomistic Modelling on Different Scales. *Prog. Energy* **2022**, *4* (1), No. 012002.

(32) Wang, Q.; Mariyappan, S.; Rousse, G.; Morozov, A. V.; Porcheron, B.; Dedryvère, R.; Wu, J.; Yang, W.; Zhang, L.; Chakir, M.; Avdeev, M.; Deschamps, M.; Yu, Y.-S.; Cabana, J.; Doublet, M.-L.; Abakumov, A. M.; Tarascon, J.-M. Unlocking Anionic Redox Activity in O3-Type Sodium 3d Layered Oxides via Li Substitution. *Nat. Mater.* **2021**, *20* (3), 353−361.

(33) Ben Yahia, M.; Vergnet, J.; Saubanère, M.; Doublet, M.-L. Unified Picture of Anionic Redox in Li/Na-Ion Batteries. *Nat. Mater.* **2019**, *18* (5), 496−502.

(34) Zhao, C.; Yao, Z.; Wang, J.; Lu, Y.; Bai, X.; Aspuru-Guzik, A.; Chen, L.; Hu, Y.-S. Ti Substitution Facilitating Oxygen Oxidation in Na$_2$/3Mg$_1$/3Ti$_1$/6Mn$_1$/2O$_2$ Cathode. *Chem.* **2019**, *5* (11), 2913−2925.

(35) Seo, D.-H.; Lee, J.; Urban, A.; Malik, R.; Kang, S.; Ceder, G. The Structural and Chemical Origin of the Oxygen Redox Activity in Layered and Cation-Disordered Li-Excess Cathode Materials. *Nat. Chem.* **2016**, *8* (7), 692−697.

(36) Massaro, A.; Muñoz-García, A. B.; Prosini, P. P.; Gerbaldi, C.; Pavone, M. Unveiling Oxygen Redox Activity in P2-Type Na$_x$Ni$_0.25$Mn$_0.68$O$_2$ High-Energy Cathode for Na-Ion Batteries. *ACS Energy Lett.* **2021**, *6* (7), 2470−2480.

(37) Massaro, A.; Langella, A.; Muñoz-García, A. B.; Pavone, M. First-principles Insights on Anion Redox Activity in Na x Fe 1/8 Ni 1/8 Mn 3/4 O 2: Toward Efficient High-energy Cathodes for Na-ion Batteries. *J. Am. Ceram. Soc.* **2023**, *106* (1), 109−119.

(38) Massaro, A.; Langella, A.; Gerbaldi, C.; Elia, G. A.; Muñoz-García, A. B.; Pavone, M. Ru-Doping of P2-Na$_x$Mn$_0.75$Ni$_0.25$O$_2$-Layered Oxides for High-Energy Na-Ion Battery Cathodes: First-Principles Insights on Activation and Control of Reversible Oxide Redox Chemistry. *ACS Appl. Energy Mater.* **2022**, *5* (9), 10721−10730.

(39) Lewandowski, A.; Świderska-Mocek, A. Ionic Liquids as Electrolytes for Li-Ion Batteries—An Overview of Electrochemical Studies. *J. Power Sources* **2009**, *194* (2), 601−609.

(40) Armand, M.; Endres, F.; MacFarlane, D. R.; Ohno, H.; Scrosati, B. Ionic-Liquid Materials for the Electrochemical Challenges of the Future. *Nat. Mater.* **2009**, *8* (8), 621−629.

(41) Marcus, Y. The Properties of Ions Constituting Ionic Liquids. *Ionic Liquid Properties: From Molten Salts to RTILs*. Springer 2016. pp. 7-24

(42) Brutti, S.; Simonetti, E.; De Francesco, M.; Sarra, A.; Paolone, A.; Palumbo, O.; Fantini, S.; Lin, R.; Falgayrat, A.; Choi, H.; Kuenzel, M.; Passerini, S.; Appetecchi, G. B. Ionic Liquid Electrolytes for High-Voltage. *Lithium-Ion Batteries. J. Power Sources* **2020**, *479*, No. 228791.

(43) Kerner, M.; Plylahan, N.; Scheers, J.; Johansson, P. Ionic Liquid Based Lithium Battery Electrolytes: Fundamental Benefits of Utilising Both TFSI and FSI Anions? *Phys. Chem. Chem. Phys.* **2015**, *17* (29), 19569−19581.

(44) Zhang, H.; Feng, W.; Nie, J.; Zhou, Z. Recent Progresses on Electrolytes of Fluorosulfonimide Anions for Improving the Performances of Rechargeable Li and Li-Ion Battery. *J. Fluor. Chem.* **2015**, *174*, 49−61.

(45) Wang, X.; Salari, M.; Jiang, D.; Chapman Varela, J.; Anasori, B.; Wesolowski, D. J.; Dai, S.; Grinstaff, M. W.; Gogotsi, Y. Electrode Material−Ionic Liquid Coupling for Electrochemical Energy Storage. *Nat. Rev. Mater.* **2020**, *5* (11), 787−808.

(46) Kohn, W.; Sham, L. J. Self-Consistent Equations Including Exchange and Correlation Effects. *Phys. Rev.* **1965**, *140* (4A), A1133−A1138.

(47) Hohenberg, P.; Kohn, W. Inhomogeneous Electron Gas. *Phys. Rev.* **1964**, *136* (3B), B864−B871.

(48) Anisimov, V. I.; Zaanen, J.; Andersen, O. K. Band Theory and Mott Insulators: Hubbard U Instead of Stoner I. *Phys. Rev. B* **1991**, *44* (3), 943−954.

(49) Kresse, G.; Furthmüller, J. Efficient Iterative Schemes for Ab Initio Total-Energy Calculations Using a Plane-Wave Basis Set. *Phys. Rev. B* **1996**, *54* (16), 11169−11186.

(50) Blöchl, P. E. Projector Augmented-Wave Method. *Phys. Rev. B* **1994**, *50* (24), 17953−17979.

(51) Perdew, J. P.; Burke, K.; Ernzerhof, M. Generalized Gradient Approximation Made Simple. *Phys. Rev. Lett.* **1996**, *77* (18), 3865−3868.

(52) Tolba, S. A.; Gameel, K. M.; Ali, B. A.; Almossalami, H. A.; Allam, N. K.The DFT+U: Approaches, Accuracy, and Applications. In *Density Functional Calculations - Recent Progresses of Theory and Application*; InTech, 2018; pp 3−30. DOI: 10.5772/intechopen.72020.

(53) Grimme, S.; Antony, J.; Ehrlich, S.; Krieg, H. A Consistent and Accurate Ab Initio Parametrization of Density Functional Dispersion Correction (DFT-D) for the 94 Elements H-Pu. *J. Chem. Phys.* **2010**, *132* (15), No. 154104.

(54) Barone, V.; Casarin, M.; Forrer, D.; Pavone, M.; Sambi, M.; Vittadini, A. Role and Effective Treatment of Dispersive Forces in

Materials: Polyethylene and Graphite Crystals as Test Cases. *J. Comput. Chem.* **2009**, *30* (6), 934−939.

(55) Wang, Q.-C.; Meng, J.-K.; Yue, X.-Y.; Qiu, Q.-Q.; Song, Y.; Wu, X.-J.; Fu, Z.-W.; Xia, Y.-Y.; Shadike, Z.; Wu, J.; Yang, X.-Q.; Zhou, Y.-N. Tuning P2-Structured Cathode Material by Na-Site Mg Substitution for Na-Ion Batteries. *J. Am. Chem. Soc.* **2019**, *141* (2), 840−848.

(56) Zunger, A.; Wei, S.-H.; Ferreira, L. G.; Bernard, J. E. Special Quasirandom Structure. *Phys. Rev. Lett.* **1990**, *65* (3), 353−356.

(57) Mayer, J. E.; Montroll, E. Molecular Distributions. *J. Chem. Phys.* **1941**, *9*, 2−16.

(58) Van de Walle, A.; Asta, M.; Ceder, G. The Alloy Theoretic Automated Toolkit: A User Guide. *Calphad Comput. Coupling Phase Diagrams Thermochem.* **2002**, *26* (4), 539−553.

(59) Fielden, R.; Obrovac, M. N. Investigation of the $NaNi_xMn_{1-x}O_2$ ($0 \leq x \leq 1$) System for Na-Ion Battery Cathode Materials. *J. Electrochem. Soc.* **2015**, *162* (3), A453−A459.

(60) Falco, M.; Lingua, G.; Destro, M.; Silvestri, L.; Meligrana, G.; Lin, R.; Fantini, S.; Maresca, G.; Paolone, A.; Brutti, S.; Appetecchi, G. B.; Elia, G. A.; Gerbaldi, C. An Electrochemical Compatibility Investigation of RTIL-Based Electrolytes with Si-Based Anodes for Advanced Li-Ion Batteries. *Mater. Today Sustain.* **2023**, *21*, No. 100299.

(61) Langella, A.; Massaro, A.; Muñoz-García, A. B.; Pavone, M. First-Principles Insights on Solid-State Phase Transitions in P2-Na_xMnO_2-Based High Energy Cathode during Na-Ion Battery Operations. *Chem. Mater.* **2024**, *36* (5), 2370−2379.

(62) Bai, Q.; Yang, L.; Chen, H.; Mo, Y. Computational Studies of Electrode Materials in Sodium-Ion Batteries. *Adv. Energy Mater.* **2018**, *8* (17), No. 1702998.

(63) Wang, K.; Wu, Z.-G.; Melinte, G.; Yang, Z.-G.; Sarkar, A.; Hua, W.; Mu, X.; Yin, Z.-W.; Li, J.-T.; Guo, X.-D.; Zhong, B.-H.; Kübel, C. Preparation of Intergrown P/O-Type Biphasic Layered Oxides as High-Performance Cathodes for Sodium Ion Batteries. *J. Mater. Chem. A* **2021**, *9* (22), 13151−13160.

(64) Delmas, C.; Carlier, D.; Guignard, M. The Layered Oxides in Lithium and Sodium-Ion Batteries: A Solid-State Chemistry Approach. *Adv. Energy Mater.* **2021**, *11* (2), No. 2001201.

(65) Karuppasamy, K.; Theerthagiri, J.; Vikraman, D.; Yim, C.-J.; Hussain, S.; Sharma, R.; Maiyalagan, T.; Qin, J.; Kim, H.-S. Ionic Liquid-Based Electrolytes for Energy Storage Devices: A Brief Review on Their Limits and Applications. *Polymers (Basel).* **2020**, *12* (4), 918.

(66) Giffin, G. A. Ionic Liquid-Based Electrolytes for "beyond Lithium" Battery Technologies. *J. Mater. Chem. A* **2016**, *4* (35), 13378−13389.

(67) Ding, Y.; Wang, S.; Sun, Y.; Liu, Q.; An, Q.; Guo, H. Layered Cathode-$Na_{0.67}Li_{0.15}Ni_{0.18}Mg_{0.02}Mn_{0.8}O_2$ with P2/O3 Hybrid Phase for High-Performance Na-Ion Batteries. *J. Alloys Compd.* **2023**, *939*, No. 168780.

(68) Wang, C.; Liu, L.; Zhao, S.; Liu, Y.; Yang, Y.; Yu, H.; Lee, S.; Lee, G.-H.; Kang, Y.-M.; Liu, R.; Li, F.; Chen, J. Tuning Local Chemistry of P2 Layered-Oxide Cathode for High Energy and Long Cycles of Sodium-Ion Battery. *Nat. Commun.* **2021**, *12* (1), 2256.

(69) Ponti, G.; Palombi, F.; Abate, D.; Ambrosino, F.; Aprea, G.; Bastianelli, T.; Beone, F.; Bertini, R.; Bracco, G.; Caporicci, M.; Calosso, B.; Chinnici, M.; Colavincenzo, A.; Cucurullo, A.; Dangelo, P.; De Rosa, M.; De Michele, P.; Funel, A.; Furini, G.; Giammattei, D.; Giusepponi, S.; Guadagni, R.; Guarnieri, G.; Italiano, A.; Magagnino, S.; Mariano, A.; Mencuccini, G.; Mercuri, C.; Migliori, S.; Ornelli, P.; Pecoraro, S.; Perozziello, A.; Pierattini, S.; Podda, S.; Poggi, F.; Quintiliani, A.; Rocchi, A.; Scio, C.; Simoni, F.; Vita, A.The Role of Medium Size Facilities in the HPC Ecosystem: The Case of the New CRESCO4 Cluster Integrated in the ENEAGRID Infrastructure. In *2014 International Conference on High Performance Computing & Simulation (HPCS)*; IEEE, 2014; pp 1030−1033. DOI: 10.1109/HPCSim.2014.6903807.